Supplementary Materials for

Intercalated montmorillonite fabricating highly-conductive and overall-stable solid composite electrolyte for advanced lithium metal battery

Yan Yuan[1*], Xinyi Dong[1], Yaxin Kong[1], Wenzhi Liang[1], Jiaxin Luo[1], Zeyu Li[1], Hai Lu[2*]

[1]School of Metallurgical Engineering, Xi'an University of Architecture and Technology, Xi'an 710055, China

[2]School of Materials Science and Engineering, Xi'an University of Science and Technology, Xi'an 710054, China

[*] Corresponding author (Y. Yuan): Tel.: +86 29 82202923

E-mail address: lingyi21@126.com

[*] Corresponding author (H. Lu): Tel.: +86 29 85587373

E-mail address: luhai@xust.edu.cn

Supplementary Notes

Materials characterizations

The crystal structure of the sample was determined by X-ray diffraction (XRD, Rigaku SmartLab SE). After baseline correction of the XRD patterns, the crystallinity values of different SCEs were calculated by integrating the areas of all crystalline peaks and amorphous peaks. Fourier transform infrared spectroscopy (FTIR, Thermo Fisher Scientific Nicolet iS20) was employed to investigate the functional structures of the samples. The surface morphology were observed by scanning electron microscopy (SEM, CLARA) coupled with Energy Dispersive X-ray Spectroscopy (EDS) for elemental analysis. The specific surface area and pore size distribution was analyzed by Brunauer-Emmett-Teller method (BET, Micromeritics ASAP 2460). The thermal stability of the SCE was examined by thermogravimetric analysis (TGA 550) from room temperature to 800 °C at a heating rate of 20 °C min^{-1} under a nitrogen atmosphere. Differential scanning calorimetry (DSC) analysis was also performed using a Netzsch DSC 200F3. X-ray photoelectron spectroscopy (XPS, Thermo Scientific K-Alpha) was used to identify surface species on the collected electrodes. All binding energy values were calibrated with C 1s peak at 284.8 eV.

Computational methods

Density functional theory (DFT) calculations were performed using the CASTEP package within Materials Studio. The electronic exchange-correlation interactions were described using generalized gradient approximation (GGA) with Perdew-Burke-Ernzerhof (PBE) functional. A plane-wave energy cutoff of 800 eV was employed. Geometry optimizations were conducted to minimize the total energy using a 4×2×1 k-point mesh sampling and L-BFGS (Limited-memory Broyden–Fletcher–Goldfarb–Shanno) algorithm. The convergence criteria for the geometry optimization were set as follows: the force on each atom during structural relaxation was less than 0.005 eV $Å^{-1}$, and the total energy change per atom was below 10^{-6} eV $atom^{-1}$. After geometry optimization of MMT, THF and DMSO molecules were introduced into the model to calculate the adsorption energy (E_{ads}) by the following equation:

$$E_{ads}=E_{total}-E_{catalyst}-E_{slab}$$

Where E_{total}, $E_{catalyst}$, and E_{slab} represent the total energy of the adsorption system, the energy of pristine MMT, and the energy of an isolated THF or DMSO molecule, respectively.

Geometry optimization for energy minimization was carried out using a DND basis set with a global orbital cutoff of 5.5 Å and a 4×2×1 k-point mesh. The convergence criteria for geometry optimization were set as follows: energy change < 1×10^{-5}Ha, maximum force < 0.002 Ha/Å, and maximum displacement < 0.005 Å.

Supplementary Figures

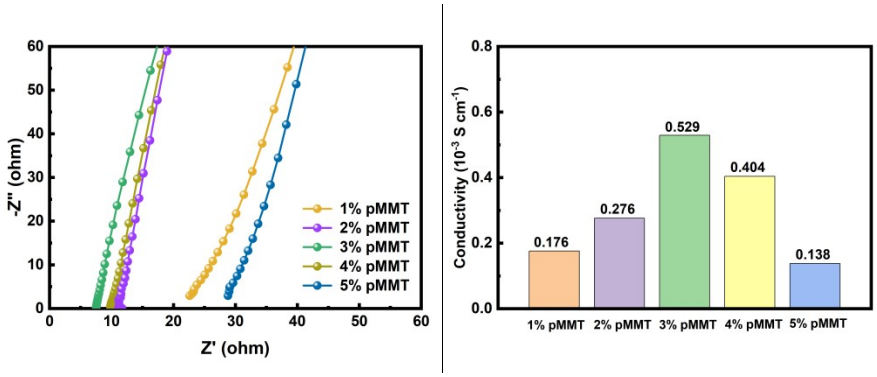

Figure S1 EIS plots of SS|SS symmetrical cells and calculated ionic conductivity of the SCEs at different amounts of pMMT

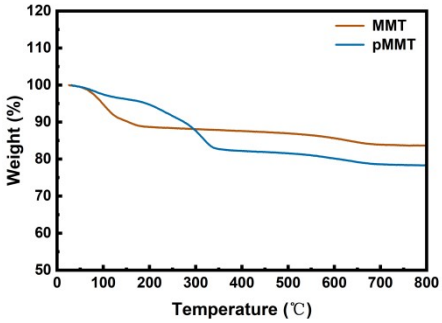

Figure S2 TGA curves of MMT and pMMT

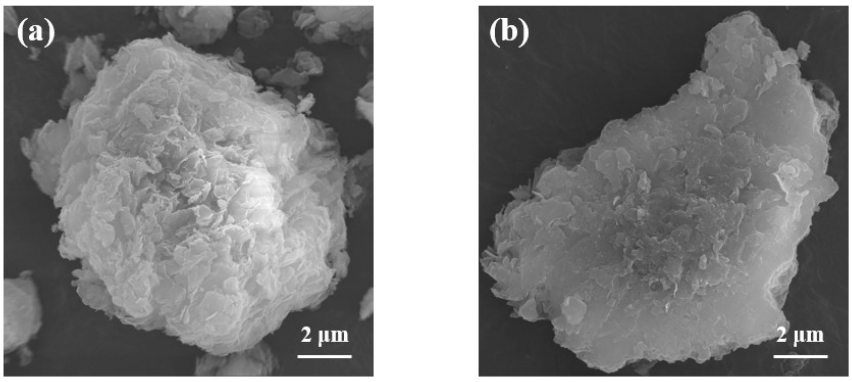

Figure S3 SEM images of (a) MMT and (b) pMMT

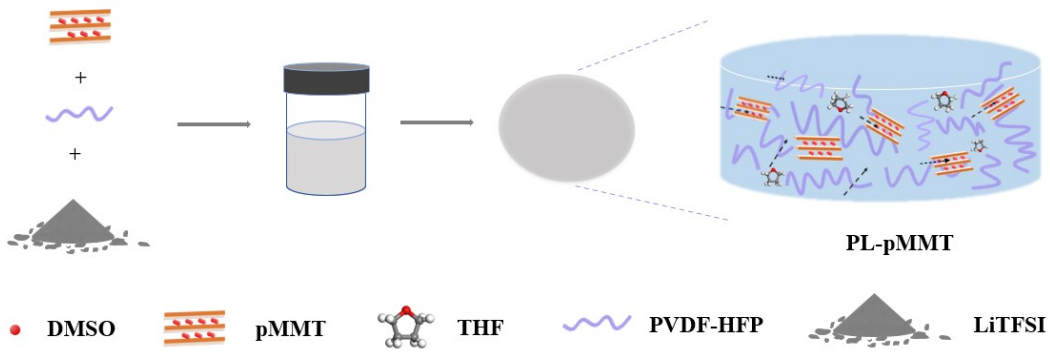

Figure S4 Schematic illustration of preparation process of PL-pMMT

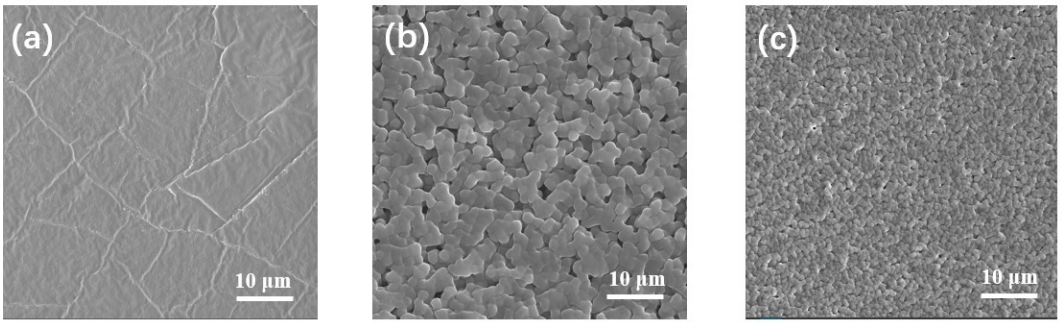

Figure S5 SEM images of (a) PL, (b) PL-MMT and (c) PL-pMMT

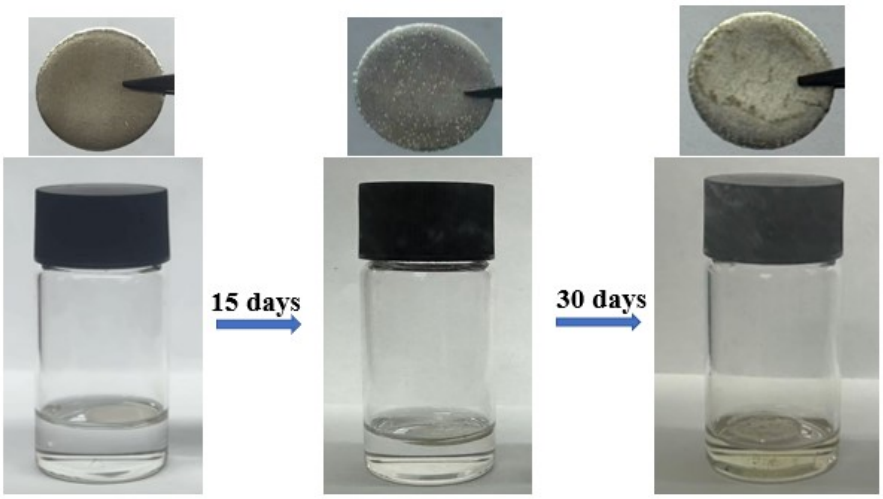

Figure S6 Corrosion visualization of THF solvent towards Li metal. Obvious surface corrosion was observed after Li metal was immersed in THF for 30 days

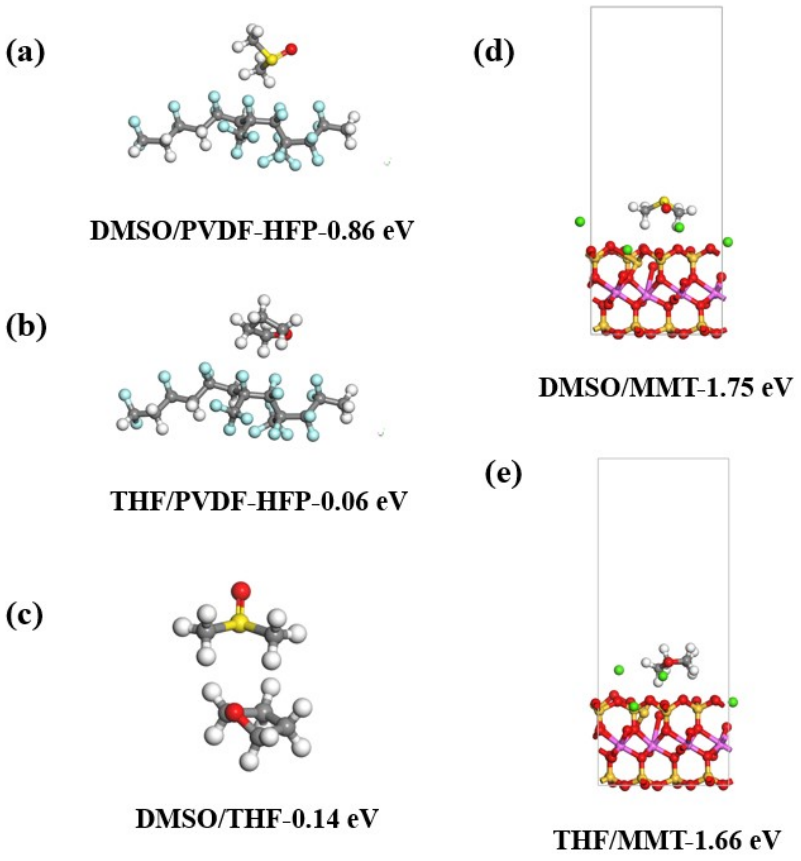

Figure S7 Adsorption configurations calculated by DFT

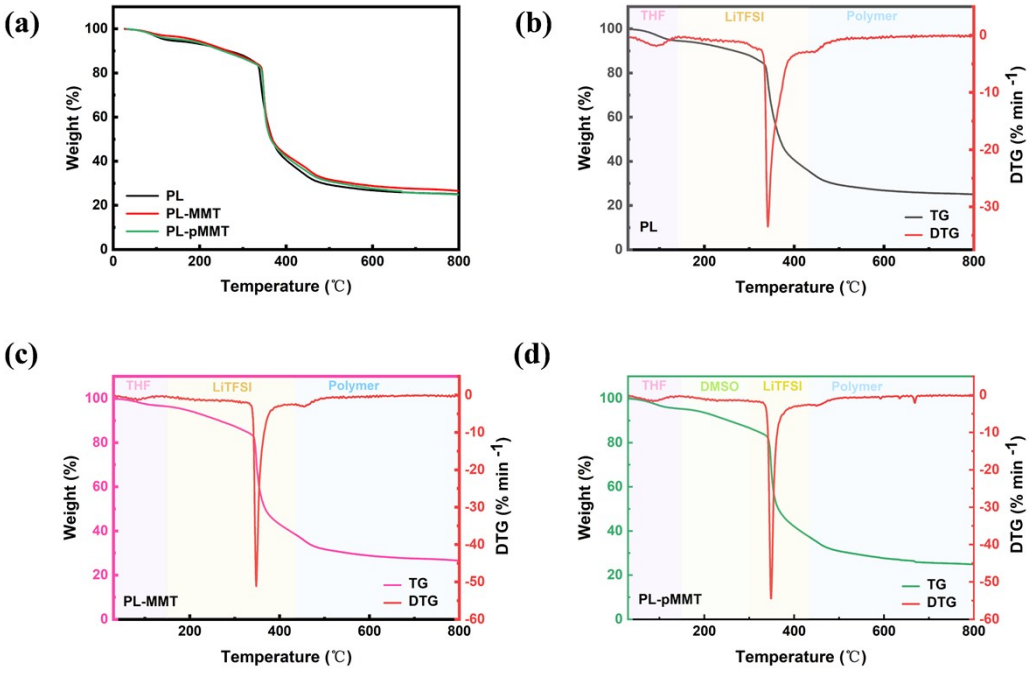

Figure S8 TG-DTG curves of various SCEs

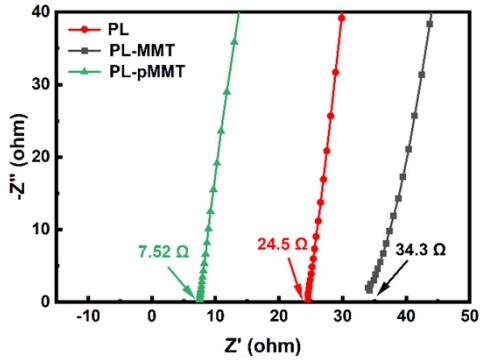

Figure S9 EIS plots of symmetrical stainless steel cell in various SCEs at room temperature

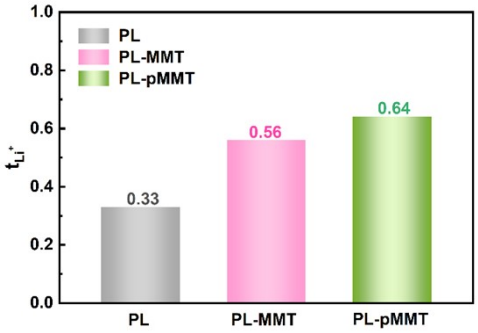

Figure S10 Li^+ transference numbers of PL, PL-MMT and PL-pMMT

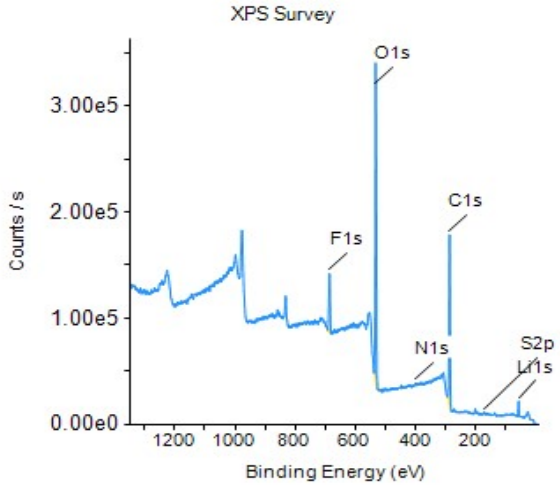

Figure S11 XPS survey spectrum of PL membrane

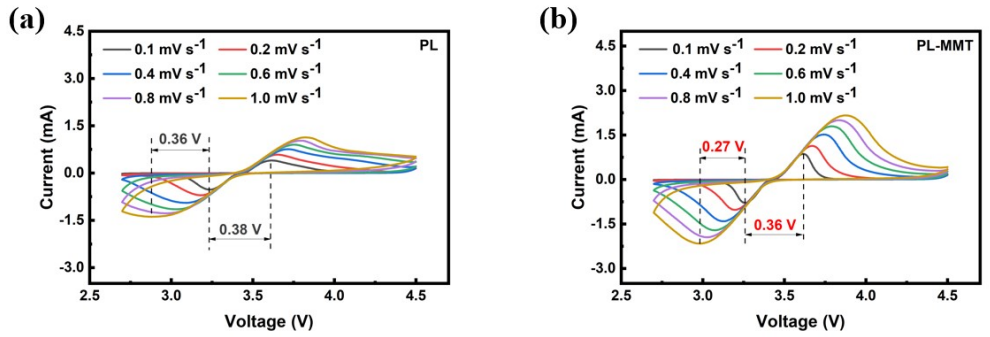

Figure S12 CV curves of LFP|PL|Li and LFP|PL-MMT|Li cells at various scan rates

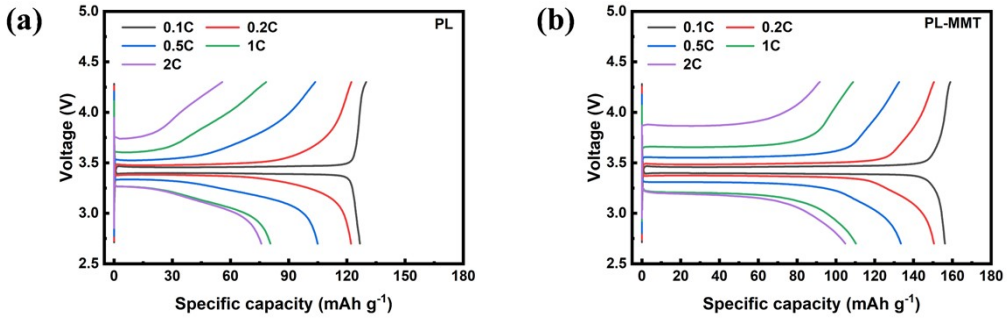

Figure S13 Charge-discharge profiles of LFP|PL|Li and LFP|PL-MMT|Li cells

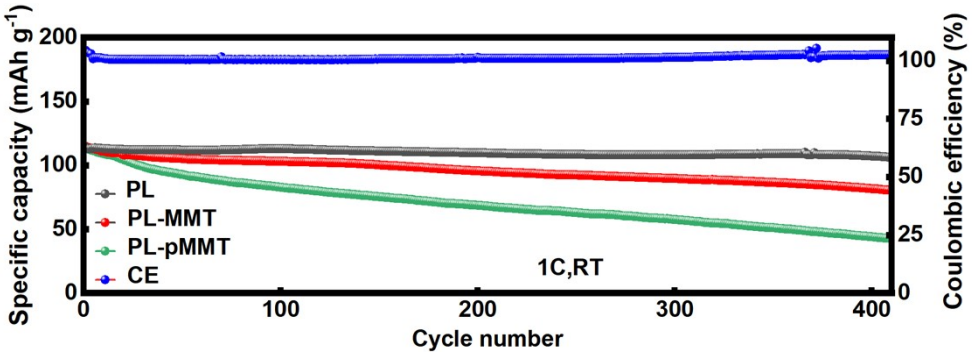

Figure S14 Cycling performance of the LFP|Li cells at 1C

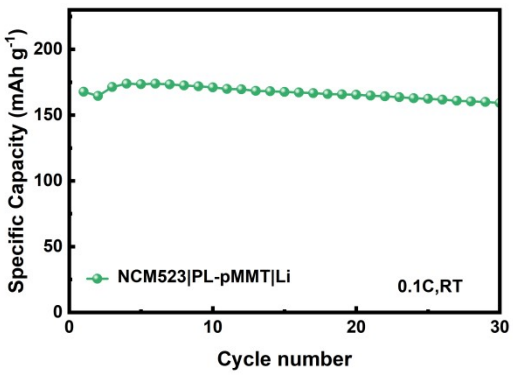

Figure S15 Cycling performance of the NCM523|PL-pMMT|Li cell at 0.1C

Supplementary Tables

Table S1 Specific surface area and pore parameters of MMT and pMMT

	MMT	pMMT
Specific surface area ($m^2\ g^{-1}$)	58.43	28.91
Micropore area ($m^2\ g^{-1}$)	12.01	5.49
Micropore volume ($cm^3\ g^{-1}$)	0.005	0.002
Average pore diameter (nm)	9.73	12.85